Hindawi Publishing Corporation
International Journal of Chemical Engineering
Volume 2015, Article ID 750689, 9 pages
http://dx.doi.org/10.1155/2015/750689

Research Article

Synthesis of CuNi/C and CuNi/γ-Al_2O_3 Catalysts for the Reverse Water Gas Shift Reaction

Maxime Lortie,[1,2] Rima Isaifan,[1,2] Yun Liu,[1] and Sander Mommers[1]

[1]*Chemical and Biological Engineering, University of Ottawa, Ottawa, ON, Canada K1N 6N5*
[2]*Centre for Catalysis Research and Innovation, University of Ottawa, Ottawa, ON, Canada K1N 6N5*

Correspondence should be addressed to Maxime Lortie; m.lortie90@gmail.com

Received 6 October 2014; Revised 8 February 2015; Accepted 9 February 2015

Academic Editor: Donald L. Feke

A new polyol synthesis method is described in which CuNi nanoparticles of different Cu/Ni atomic ratios were supported on both carbon and gamma-alumina and compared with Pt catalysts using the reverse water gas shift, RWGS, reaction. All catalysts were highly selective for CO formation. The concentration of CH_4 was less than the detection limit. Cu was the most abundant metal on the CuNi alloy surfaces, as determined by X-ray photoelectron spectroscopy, XPS, measurements. Only one CuNi alloy catalyst, $Cu_{50}Ni_{50}$/C, appeared to be as thermally stable as the Pt/C catalysts. After three temperature cycles, from 400 to 700°C, the CO yield at 700°C obtained using the $Cu_{50}Ni_{50}$/C catalyst was comparable to that obtained using a Pt/C catalyst.

1. Introduction

The carbon dioxide hydrogenation reaction has been proposed for use with carbon capture technologies for the production of industrially viable chemicals, such as long chain hydrocarbons, methanol, formic acid, and carbon monoxide [1, 2]. When cofeeding CO_2 and H_2 over a hydrogenation catalyst, there are two main hydrogenation processes that can take place, the reverse water gas shift reaction

$$CO_2 + H_2 = CO + H_2O \quad (1)$$

and the subsequent hydrogenation of CO to either hydrocarbons or alcohols, depending on the values of x, y, and z in

$$x\mathrm{CO} + \left(x - z + \frac{y}{2}\right)\mathrm{H_2} = \mathrm{C_XH_YO_Z} + (x - z)\,\mathrm{H_2O} \quad (2)$$

One of the reactions in (2), the hydrogenation of CO to methane, is of particular interest in this study:

$$CO + 2H_2 = CH_4 + H_2O \quad (3)$$

When CO is selectively formed via (1) and mixed with H_2, the resulting syngas can be a feed-stock for the Fischer Tropsch process [2] that produces liquid fuels. In contrast CH_4 formed via (3) is an undesirable by-product that is not convertible to liquid fuels in a Fischer Tropsch process.

Wang et al. [1] have recently reviewed catalysts for the RWGS reaction. They reported that noble metals have been studied and shown to be among the best catalysts for the RWGS reaction because they generally promote H_2 dissociation. Among noble metals used for the RWGS reaction, platinum (Pt) has received considerable attention. It was found to produce high CO yields [3–5]. In addition, Pekridis et al. [6] tested the electrokinetics of the RWGS reaction in solid oxide fuel cells containing a Pt/YSZ catalyst. The Pt/YSZ catalyst was found to be stable at high temperatures and the cell achieved a maximum power density of 9 mW/cm^2 [6]. In spite of the recognized performance of noble metals as catalysts for the RWGS reaction, their main drawback is their high cost that limits their commercial application.

Transition metals such as copper (Cu), nickel (Ni), and iron (Fe) are promising alternatives to noble metal catalysts for the RWGS reaction. Both copper and nickel based catalysts have shown good conversion for the WGS reaction as well as the RWGS reaction [7–12]. Chen et al. [7] investigated Cu nanoparticles ranging in size from 2.4 to 3.4 nm and found that the catalyst becomes unstable at higher temperatures [13]. These researchers [14] also added

Fe to Cu in an attempt to stabilize the catalyst. Although Fe alone had poor conversions, Fe stabilized the Cu catalyst for 120 h and caused an increase in conversion of approximately 7% at 600°C. On the other hand, the Cu catalyst without the iron stabilizer was deactivated rapidly and reached zero conversion after 120 hours.

Similar research was performed by Chen et al. [15] using Ni catalysts. Ni alone showed high selectivity towards methane. When they added potassium to a Ni/γ-Al_2O_3 catalyst they reported higher selectivity towards CO even though they did not notice an increase in CO_2 conversion. However with the potassium promoter they noticed the formation of coke.

Y. Liu and D. Liu [16] studied a Ni-Cu catalyst that was prepared by immersing gamma-alumina (γ-Al_2O_3) in an aqua ammonia solution of nickel nitrate and copper nitrate. Their catalysts were not selective in that they reported large yields of both CH_4 and CO. They interpreted their results as CO_2 being adsorbed on Cu and H_2 being adsorbed on Ni.

The polyol synthesis method has been used extensively in the past for the synthesis of metal particles from a metal salt precursor [$Cu(NO_3)_2$ or $Ni(NO_3)_2$ represented here as $Me(NO_3)_2$]. Bonet et al. [17, 18] indicated that the overall reactions at 180°C included the following reactions to form acetic acid, glycolaldehyde, and glycolic acid:

$$(CH_2OH)-(CH_2OH) + Me(NO_3)_2 \longrightarrow CH_3COOH + 2HNO_3 + Me^0 \quad (4)$$

$$(CH_2OH)-(CH_2OH) + Me(NO_3)_2 \longrightarrow (CH_2OH)-(CHO) + 2HNO_3 + Me^0 \quad (5)$$

$$(CH_2OH)-(CH_2OH) + H_2O + 2Me(NO_3)_2 \longrightarrow (CH_2OH)-(COOH) + 4HNO_3 + 2Me^0 \quad (6)$$

Bock et al. [19] found that oxalic acid, HOOC–COOH, is also formed and suggested that the majority of the metal is formed by the oxidation of ethylene glycol to glycolic acid. At the boiling point of ethylene glycol, 196°C, Poul et al. [17] indicated that the overall reactions included the formation of diacetyl:

$$2(CH_2OH)-(CH_2OH) + Me(NO_3)_2 \longrightarrow (CH_3CO)-(CH_3CO) + 2H_2O + 2HNO_3 + Me^0 \quad (7)$$

where Me^0 represents either copper or nickel in the metallic state. Poul et al. [17] also commented on the reaction mechanism and indicated that intermediate solid phases (metal glycolates) precipitate before the metal powder is formed. Bonet et al. [18] indicated that oxidation products containing carboxylic acids act as stabilizers for metal colloid particles. Specifically they indicated that glycolate anions, the deprotonated form of glycolic acid, are good stabilizers for colloidal metal particles and that their concentration increases when the pH is greater than 6. In their work, they increased the pH by the addition of NaOH and reported that PtRu bimetallic nanoparticle sizes decreased when the pH was increased. Their explanation of glycolate anions on the exterior of the metal particles preventing metal colloid agglomeration seems to be consistent with their nanoparticle size results. The polyol synthesis method has become known for its simplicity and accurate control of particle size [17, 18].

Other researchers [16, 18, 20] have also used the polyol synthesis method to obtain bimetallic particles. When alloying two metals together, the resulting reaction properties can often be enhanced compared to the pure metal. In the past both Cu and Ni have been alloyed with other metals to form alloys. For instance, Viau et al. [20] prepared Co-Ni and Fe-Ni particles using the polyol synthesis method.

Bonet et al. [18] used a polyol synthesis method to obtain CuNi particles. When nickel carbonate and copper carbonate were used at 140°C they obtained a CuNi powder composed of both a Ni rich CuNi solid solution and a Cu rich CuNi solid solution. When the carbonates were used at 196°C they obtained a CuNi powder composed of a Cu rich CuNi solid solution and a solid Ni metal phase. They noted that the reduction temperature for Cu is less than that for Ni. Their particles had a particle size of 140 nm. They did not report any reaction results.

In this work base metal CuNi nanoparticle catalysts were prepared by a new synthesis technique and used for the RWGS reaction. Cu was chosen because it is selective for the formation of CO [16], although it is unstable (sinters) at the higher temperatures where the equilibrium for the RWGS reaction is more favourable. Ni was chosen because it also produces CO [15] although it also can form unwanted by-products, CH_4, and coke.

The main objective of this investigation was to obtain physical characterization of the CuNi nanocatalyst and to use this catalyst in the RWGS reaction. The results obtained with the CuNi catalyst were then compared to Pt nanoparticle catalysts that were already synthesized and tested using a variety of reactions: ethylene oxidation [21], CO oxidation [22], and toluene oxidation [23]. These Pt catalysts are considered to be among the best catalysts for the RWGS reaction because they achieve reaction equilibrium at some conditions. Another purpose of the investigation was to determine if sintering of pure Cu could be prevented by the addition of Ni in the same way that it was prevented by the addition of Fe [14]. In what follows, we report CuNi catalyst compositions that promote CO formation and inhibit CH_4 formation at specific reaction conditions.

2. Experiment

2.1. Catalyst Preparation. CuNi nanoparticles were synthesised using a modified polyol technique. Nickel nitrate ($Ni(NO_3)_2$) (hexahydrate 99.999% metal basis, Alfa Aesar) was dissolved in ethylene glycol (anhydrous 99.8%, Sigma Aldrich). Next, an increase in pH to 11 was achieved by sodium hydroxide (NaOH) pellets (EM Science, ACS grade) to obtain the first solution. Separately, copper nitrate ($Cu(NO_3)_2$) (hexahydrate 99.999% metal basis, Alfa Aesar) was also dissolved in ethylene glycol. Its pH was also increased to

Table 1: Catalyst physical characteristics.

Catalyst	Metal loading (wt%)	XRD crystalline size (nm)	Typical particle size (nm)
Pt/C	1	3.8	2.8
Pt/γ-Al_2O_3			N/A
$Cu_{80}Ni_{20}$/C	10	30.2	64.4
$Cu_{80}Ni_{20}$/γ-Al_2O_3			N/A
$Cu_{50}Ni_{50}$/C	10	24	53.4
$Cu_{50}Ni_{50}$/γ-Al_2O_3			N/A
$Cu_{20}Ni_{80}$/C	10	16.7	41.1
$Cu_{20}Ni_{80}$/γ-Al_2O_3			N/A

ll using NaOH pellets to obtain a second solution. Solution 1 was then refluxed and stirred at 196°C. Once the temperature reached 196°C, the second solution, which was at room temperature, was added to the reflux. The mixture was left to reflux at 196°C for 30 minutes and then cooled. The colloidal particles were then stored in solution at room temperature.

A wet impregnation technique was used to deposit the colloidal particles on supports. The powdered support was first placed into a beaker. Then, a specific amount of colloidal particles was injected in the powder. A nominal amount of 10 wt% of CuNi was chosen. The mixture was sonicated for 1 hour and stirred for 24 hours. The catalyst was then centrifuged and washed with deionized water several times in order to remove any salts remaining from the synthesis procedure. The supports used were carbon black (Vulcan XC-72R, Cabot Corp., specific surface area of 254 m^2/g) and gamma-alumina (Alfa Aesar, specific surface area of 120 m^2/g). A freeze dryer was used to dry the catalyst. The catalyst was finely crushed prior to all experiments.

CuNi particles of three different compositions were prepared. The combined solution for each composition was prepared with a different ratio of Solution 1 to Solution 2. The ratio was selected to obtain CuNi colloidal particles of 80 wt% Cu/20 wt% Ni (nominally $Cu_{80}Ni_{20}$), 50 wt% Cu/50 wt% Ni (nominally $Cu_{50}Ni_{50}$), and 20 wt% Cu/80 wt% Ni (nominally $Cu_{20}Ni_{80}$).

Pt nanoparticles were synthesized using a different polyol synthesis method described here [22]. In short, $PtCl_4$ was dissolved in a 0.06 M NaOH solution of ethylene glycol and refluxed at 160°C for 3 hours. The nanoparticles were then deposited on C and γ-Al_2O_3 using the same deposition technique described previously. A nominal value of 1 wt% of Pt was chosen.

2.2. Physical Characterization. Supported Pt nanoparticles were analyzed using transmission electron microscopy (TEM) with a JEOL JEM 2100F FETEM operating at 200 kV. A particle size distribution was obtained using ImageJ software. More in-depth characterisation of the Pt nanoparticle is described elsewhere [20].

Scanning electron microscopy (SEM) was conducted on carbon supported CuNi nanoparticles using a JEOL model JSM-7500F field emission scanning electron microscope, FESEM, in both lower-secondary electron image, LEI, and compositional, COMPO, modes set at a distance of 8 mm with an acceleration voltage of 5 kV. In addition, an energy-dispersive X-ray spectroscope (EDS) operating with the SEM was used to obtain a quantifiable amount of Cu and Ni in the CuNi particles.

CuNi colloidal particles were analyzed using X-ray diffraction (XRD) with a Rigaku Ultima IV diffractometer which used a Cu Kα X-ray (40 ma, 44 kV) operating with focused beam geometry and a divergence slit of 2/3 degree, a scan speed of 0.17 deg min^{-1}, and a scan step of 0.06 degrees were used while operating between 35° and 55°. Table 1 demonstrates the crystal sizes obtained through XRD.

2.3. Reaction Experiments. The performances of the supported CuNi catalysts were evaluated using the RWGS reaction. 50 mg of powdered catalyst was placed on a fritted quartz bed within a 35 mL quartz tube to act as a fixed bed reactor. A gas mixture of 1 kPa H_2 (Grade 4.0, Linde), 1 kPa CO_2 (Grade 3.0, Linde), and the balance He (Grade 4.7 Linde) flowed through the reactor at a total flow rate of 510 mL/min. The reaction was performed at atmospheric pressure using three consecutive temperature cycles. Each temperature cycle consisted of a series of experiments over the temperature range from 400°C to 700°C. Before each experiment, the temperature was held constant for 30 min. Although the same mass of catalyst was used in each experiment, the gas hourly space velocity (GHSV) was different because the supports had different bulk densities (288 g/L for the carbon support and 461 g/L for the alumina support). The GHSV values were 176000 h^{-1} and 282000 h^{-1}, respectively, for CuNi/C and CuNi/Al_2O_3 catalysts. The effluent was dehumidified by flowing through an adsorbent and was analyzed by flowing through a mass spectrometer (Ametek Proline DM 100) and a nondispersive infrared CO gas analyzer (Horiba VIA-510). Each set of experiments was repeated three times (24 hrs total) in order to examine reproducibility and stability. The yield of CO was calculated using the following formula:

$$\text{Yield of CO}\,(\%) = \frac{[\text{CO}]_{\text{OUT}}}{[\text{CO}_2]_{\text{IN}}} \times 100\%. \quad (8)$$

The mass spectrometer identified any by-products that were formed via side reactions such as CO methanation. The mass spectrometer indicated the presence of gases with a molecular weight of up to 50 atomic units and had a detection limit of 50 ppm.

3. Results and Discussion

The X-ray diffraction spectra of the CuNi nanoparticles are shown in Figure 1. The positions of the peaks for both pure Cu (2θ = 43.2, ICSD Collection Code 53246) and pure Ni (2θ = 44.6, ICSD Collection Code 43397) are shown as straight vertical lines in Figure 1. They are the X-ray reflections from the 111 crystal lattice planes. These peaks have corresponding lattice constants of 3.627 Å and 3.519 Å for pure Cu and pure Ni, respectively. The smaller peaks near 2θ values of 50.4 and 51.5 are the reflections from the 200 crystal lattice planes of Cu and Ni, respectively. No other species or oxides were identified.

There is a slight difference between the peak positions for the pure metals and the metals in the catalysts. Deviations exist because the catalysts are bimetallic solid solutions rather than pure metals. Because of these shifts, the lattice constants of each alloy are shifted. The catalyst that is nominally $Cu_{50}Ni_{50}$ in Figure 1(b) had a first 2θ peak position of 43.385 and a lattice constant of 3.612 Å which is slightly greater than the one for pure Cu. A second peak is observed near the first 2θ peak in Figure 1(b) which has a peak position of 44.346 and a lattice constant of 3.537 Å for Ni, which is slightly less than the one for pure Ni. These changes in lattice constants suggest that the two peaks represent a Cu rich alloy and a Ni rich alloy.

There is only one peak for the $Cu_{80}Ni_{20}$ catalyst in Figure 1(c). That means that all of the Ni was soluble in the Cu lattice. The single peak in Figure 1(c) is experimental evidence for a copper-rich CuNi solid solution in which the spacing between planes of the catalyst lattice is close to that of pure copper.

There are two peaks for the $Cu_{20}Ni_{80}$ catalyst in Figure 1(a). Because the first peak has a 2θ value at 43.394 and a lattice constant of 3.611 Å, close to that for pure Cu, the spacing between its planes will be similar to pure copper. Because the second peak has a 2θ value at 44.412 and a lattice constant of 3.533 Å, close to that for pure Ni, the spacing between its planes will be similar to pure nickel. Even though there is a large disparity between the bulk Cu content and the bulk Ni content of the catalyst, the two peaks appear to have similar areas. Therefore a substantial amount of Ni must be dissolved in the first Cu-like peak, and the first peak must represent a CuNi solid solution. Since the second peak has a lattice constant slightly different from pure Ni it will contain some Cu making it a Ni rich NiCu solid solution.

The observation of solid solutions is consistent with other works reported in the literature. Bonet et al. [18] synthesized CuNi particles using a similar technique. In their work they refluxed copper and nickel carbonates starting materials in ethylene glycol. After 39 hours at 140°C they observed the presence of a copper-rich solid solution, $Cu_{81}Ni_{19}$, and a Ni rich solid solution, $Ni_{86}Cu_{14}$.

The crystalline size of the synthesized nanoparticles increases with Cu content. A summary of their diameters (15–65 nm) can be found in Table 1. They were calculated from the XRD data using Scherrer's formula. The CuNi particles described by Poul et al. [17] had diameters of 250–400 nm. It is possible that the longer refluxing times and the absence of NaOH may have provided more opportunity for agglomeration.

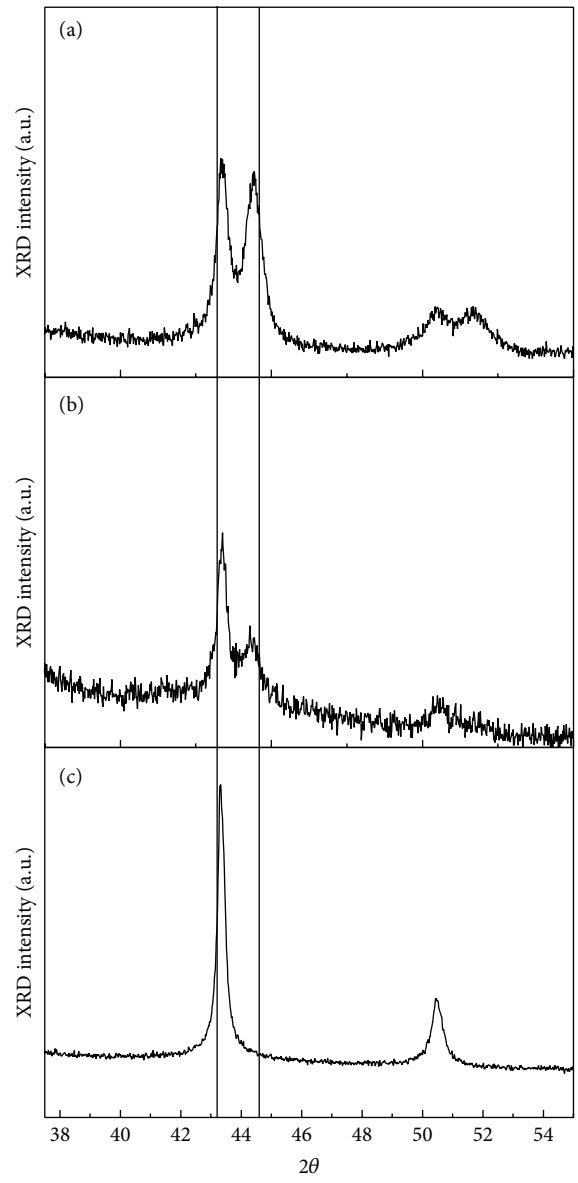

Figure 1: XRD spectra of colloidal: (a) $Cu_{20}Ni_{80}$, (b) $Cu_{50}Ni_{50}$, and (c) $Cu_{80}Ni_{20}$.

Pt/C nanoparticles characterisation can be found in [21]. In her work, Isaifan et al. demonstrate that the particles are mainly spherical with a reasonably narrow size distribution. The dispersion also appears to be relatively high. Numerical data derived from several TEM images indicated that a typical particle size for the Pt/C particles was 2.8 nm (Table 1).

An SEM image for the $Cu_{50}Ni_{50}$/C catalyst is shown in Figure 2. The particles appear to be generally spherical and to vary in size. The largest observed particle was approximately 100 nm. There are visible signs of agglomeration which is to be expected since no antiagglomerate such as polyvinylpyrrolidone (PVP) was used.

Table 2: Cu-Ni surface ratios obtained from XPS measurements.

	Theoretical bulk Cu/Ni ratio from nominal composition	Actual Surface Cu/Ni ratio from XPS	Percentage Increase
$Cu_{20}Ni_{80}$	0.25	1.2	380%
$Cu_{50}Ni_{50}$	1	2	100%
$Cu_{80}Ni_{20}$	4	4.2	5%

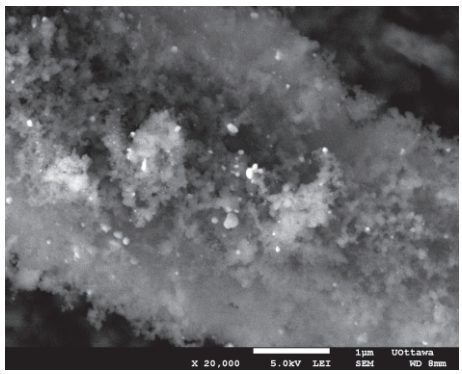

Figure 2: SEM image of a $Cu_{50}Ni_{50}$/C catalyst.

Typical particle sizes for all of the CuNi catalysts measured by SEM are listed in Table 1. In general the CuNi particle sizes are an order of magnitude larger than the Pt particle size. Since the CuNi metal loading, for example, 10 wt%, is an order of magnitude larger than the Pt loading, for example, 1 wt%, a greater extent of metal particle agglomeration might be expected for the CuNi particles.

An energy-dispersive X-ray spectroscopy, EDS, analysis was also performed on the catalyst. For example, the $Cu_{80}Ni_{20}$/C catalyst had a measured composition of 82.7 wt% Cu and 17.3 wt% Ni. The EDS measurement was repeated at two different sites on the catalyst's surface with reproducible results. That EDS result is essentially the same as the XRD composition of $Cu_{82}Ni_{18}$ that was mentioned above. Both the EDS results and the XRD results were consistent with the $Cu_{80}Ni_{20}$ nominal composition of the synthesized particles. This indicates that the synthesis method was successful in obtaining the nominal Cu : Ni ratio that was intended.

XPS measurements were performed on the CuNi/C catalysts to determine their surface compositions. The results in Table 2 show that the Cu surface concentration was greater than that of the Cu bulk concentrations for all three of the CuNi/C catalysts. Furthermore, the surface concentration of the Cu always exceeded the surface concentration of the Ni, even for the nominal $Cu_{20}Ni_{80}$/C catalyst. That result is consistent with the literature. An early report by van der Plank and Sachtler [24] indicated that Cu was the dominant species on the surface of CuNi alloys. Subsequently Watanabe et al. [25] provided definitive experimental data for the phenomenon. Later Sakurai et al. stated that the phenomenon had been conclusively shown [26].

In order to examine the physical changes of the catalyst, $Cu_{50}Ni_{50}$/C was examined by SEM and XPS before and after exposure to high temperatures and reactants. There were no visible signs of additional agglomeration or any other physical changes to the metal in comparison to the unreacted catalyst. This suggests that the catalyst is compositionally stable at temperatures of at least 700°C.

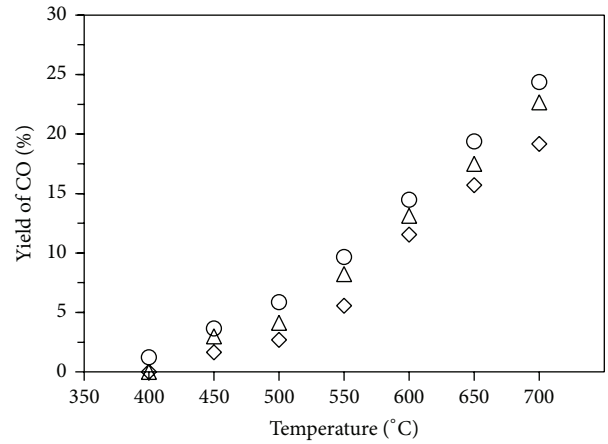

Figure 3: RWGS reaction at 1 atm, $P_{H2} = P_{CO2} = 1$ kPa, balance He, GHSV = 176000 h^{-1}, and 50 mg of catalyst: $Cu_{80}Ni_{20}$/C, 10 wt%, where ◯ = 1st cycle, △ = 2nd cycle, and ◇ = 3rd cycle.

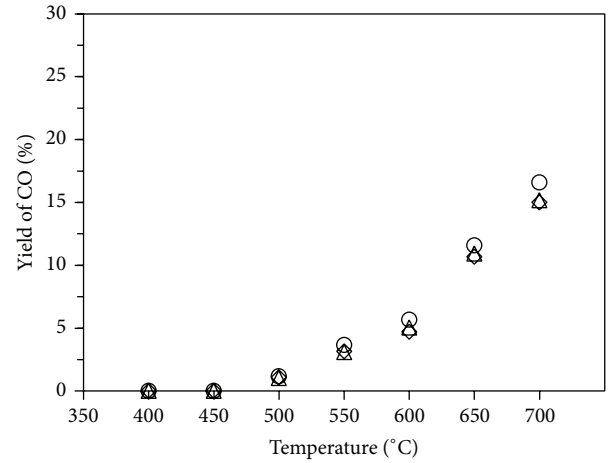

Figure 4: RWGS reaction at 1 atm, $P_{H2} = P_{CO2} = 1$ kPa, balance He, GHSV = 176000 h^{-1}, and 50 mg of catalyst: $Cu_{50}Ni_{50}$/C, 10 wt%, where ◯ = 1st cycle, △ = 2nd cycle, and ◇ = 3rd cycle.

The reverse water gas shift reaction was performed using eight different catalysts. These results can be seen in Figures 3–10. In each figure the results for the 3 consecutive temperature cycles, over the temperature range from 400°C to 700°C, are shown. Some of the CuNi catalysts showed slight deactivation between the first and second cycles and also between the second and third cycles.

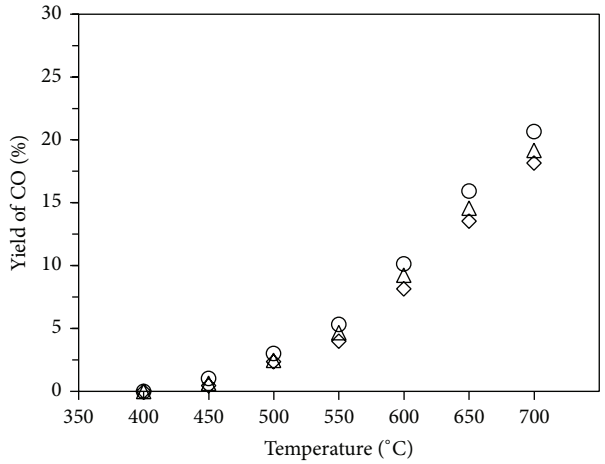

Figure 5: RWGS reaction at 1 atm, $P_{H2} = P_{CO2} = 1$ kPa, balance He, GHSV = 176000 h^{-1}, and 50 mg of catalyst: $Cu_{20}Ni_{80}$/C, 10 wt%, where ◯ = 1st cycle, △ = 2nd cycle, and ◇ = 3rd cycle.

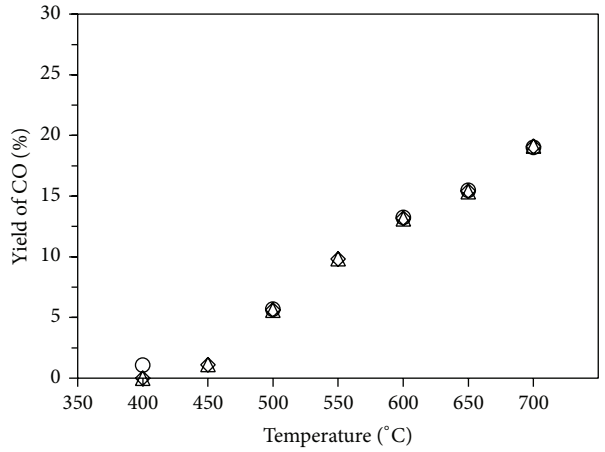

Figure 6: RWGS reaction at 1 atm, $P_{H2} = P_{CO2} = 1$ kPa, balance He, GHSV = 176000 h^{-1}, and 50 mg of catalyst: Pt/C, 1 wt%, where ◯ = 1st cycle, △ = 2nd cycle, and ◇ = 3rd cycle.

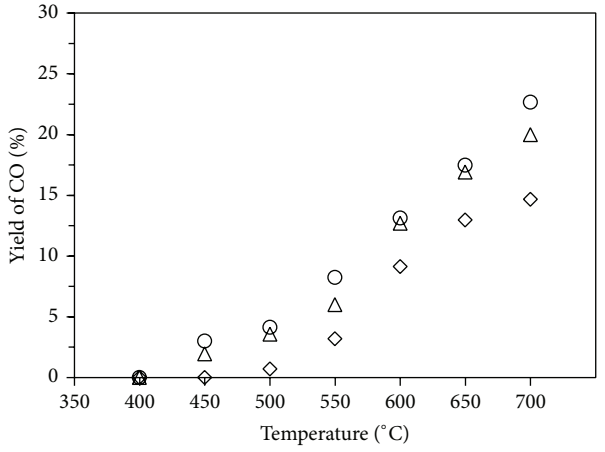

Figure 7: RWGS reaction at 1 atm, $P_{H2} = P_{CO2} = 1$ kPa, balance He, GHSV = 282000 h^{-1}, and 50 mg of catalyst: $Cu_{80}Ni_{20}/\gamma$-Al_2O_3, 10 wt%, where ◯ = 1st cycle, △ = 2nd cycle, and ◇ = 3rd cycle.

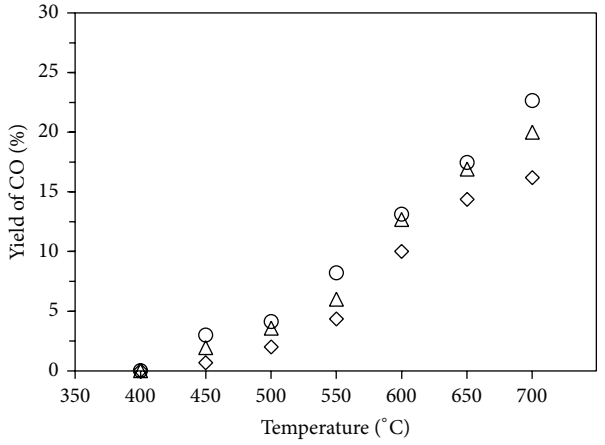

Figure 8: RWGS reaction at 1 atm, $P_{H2} = P_{CO2} = 1$ kPa, balance He, GHSV = 282000 h^{-1}, and 50 mg of catalyst: $Cu_{50}Ni_{50}/\gamma$-Al_2O_3, 10 wt%, where ◯ = 1st cycle, △ = 2nd cycle, and ◇ = 3rd cycle.

The catalysts supported on gamma-alumina, γ-Al_2O_3, are shown in Figures 7–10. In general the CO yields on the γ-Al_2O_3 supported catalyst were slightly greater than those on the carbon supported catalysts in Figures 3–6. For the first temperature cycle the CuNi metal γ-Al_2O_3 supported catalysts produced CO yields at 700°C that was 2–4% less than those produced by the Pt metal γ-Al_2O_3 supported catalyst. In addition, only the Pt metal γ-Al_2O_3 supported catalyst produced a nonzero CO yield at 400°C during the first cycle.

The only observable components in the gas stream entering the mass spectrometer were CO_2, H_2, CO, trace amounts of H_2O, and the carrier gas, He. These results indicate that CO was the main product having a typical concentration of 2000 ppm. Other products including CH_4 had concentrations less than the detection limit of the spectrometer, 50 ppm.

The absence of CH_4 in the products was a highly desirable result, since CH_4 is an undesirable by-product if syngas for a Fischer Tropsch process is the goal. Cu is known to favour CO production while CH_4 is known to form on Ni catalysts [1]. Since some of the catalysts used in this work contained 80 wt% Ni the absence of CH_4 might be considered to be inconsistent with the literature [1]. The advantage of the CuNi alloys made using this particular polyol synthesis method is that more than one-half of the surface was composed of Cu, even for catalysts consisting of 80% Ni in bulk metal, as was shown by our XPS results. Perhaps the presence of sufficient Cu on the surface may allow CO to desorb before additional hydrogenation occurs to form CH_4.

The catalysts supported on carbon are shown in Figures 3–6. $Cu_{80}Ni_{20}$/C showed the highest yield among all catalysts during the first cycle. In addition, it was the only CuNi metal carbon supported catalyst that produced a CO yield at 400°C during the first cycle. It is well known that Cu alone has better performance for the RWGS reaction than Ni [1, 16, 27] since Ni tends to further hydrogenate CO to CH_4. The increased Cu content on the surface of the $Cu_{80}Ni_{20}$

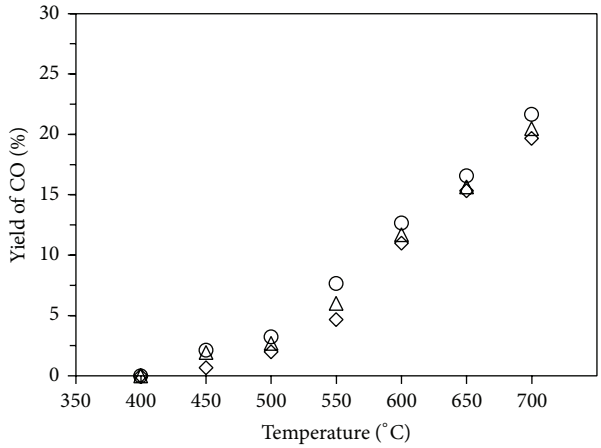

FIGURE 9: RWGS reaction at 1 atm, $P_{H2} = P_{CO2} = 1$ kPa, balance He, GHSV = 282000 h^{-1}, and 50 mg of catalyst: $Cu_{20}Ni_{80}/\gamma$-Al_2O_3, 10 wt%, where ◯ = 1st cycle, △ = 2nd cycle, and ◇ = 3rd cycle.

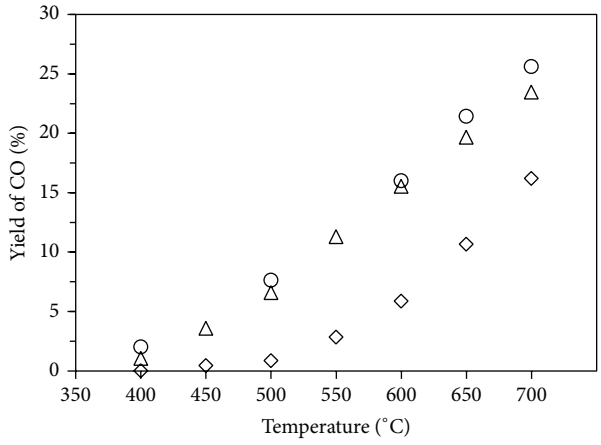

FIGURE 10: RWGS reaction at 1 atm, $P_{H2} = P_{CO2} = 1$ kPa, balance He, GHSV = 282000 h^{-1}, and 50 mg of catalyst: Pt/γ-Al_2O_3, 1 wt%, where ◯ = 1st cycle, △ = 2nd cycle, and ◇ = 3rd cycle.

catalyst seems to cause the increase in catalytic performance observed here. However, because of copper's instability at high temperatures [28], a reduction in performance was expected and is observed over time as shown in Figure 3. The yields of CO at 700°C using all the CuNi carbon supported catalysts differed from those using Pt by no more than 3%.

Deactivation was observed between the first and second temperature cycles for all of the CuNi catalysts supported on carbon. Virtually no deactivation was observed when using the Pt metal carbon supported catalyst. This suggests that the deactivation observed with the CuNi carbon supported catalyst may have been related to the CuNi metal and not to the catalyst support. The $Cu_{50}Ni_{50}$/C catalyst in Figure 4 was different from the $Cu_{20}Ni_{80}$/C and $Cu_{80}Ni_{20}$/C catalysts in that no deactivation occurred between the second and third temperature cycles. This suggests that after sufficient time-on-stream the performance of the $Cu_{50}Ni_{50}$/C may become invariant with time and that it may become a thermally stable catalyst.

Furthermore, XPS experiments of the $Cu_{50}Ni_{50}$/C showed no differences in carbon surface composition for both of the Cu and Ni atoms. These experiments suggest that coking did not occur. SEM images also showed no change in particle size either before or after testing. The sample seems to be compositionally stable throughout the experiments.

Deactivation was observed between the first and third temperature cycles for all the γ-Al_2O_3 supported catalysts, for both CuNi and Pt. The smallest extent of deactivation, 2%, was observed with the $Cu_{20}Ni_{80}\gamma$-Al_2O_3 supported catalyst. It is the CuNi catalyst with the smallest Cu content. In contrast the CO yields at 700°C for $Cu_{80}Ni_{20}$ and Pt γ-Al_2O_3 supported catalysts decreased by over 8% between the first and third temperature cycles. Conversely, no deactivation was observed for Pt metal carbon supported catalysts. This suggests that the γ-Al_2O_3 support may contribute to the deactivation. It is known [29] that as the temperature is increased above 500°C, gamma-alumina can be converted to other phases such as delta alumina, theta alumina, and alpha alumina. Alpha alumina has a much smaller surface area than gamma-alumina. The tendency of the γ-Al_2O_3 support to deactivate at high temperatures is consistent with literature data [14, 30].

Y. Liu and D. Liu [16] tested a similar catalyst having $C_{50}Ni_{50}/\gamma$-Al_2O_3 at a maximum temperature of 600°C. In their research, Y. Liu and D. Liu use a typical coimpregnation method where γ-Al_2O_3 is immersed in a solution of nickel nitrate and copper nitrate. They used twice the metal content (20 wt%) and much smaller GHSVs (much greater residence times in the reactor) and obtained CO_2 conversions that exceeded the ones being reported here. They used a catalyst preparation method that was different compared to the one used here. In fact, it did not seem to be possible to make a CuNi alloy using this technique when it was attempted in our laboratories. Perhaps that may explain why the CH_4 selectivity (e.g., 28.2%) in their work was much greater than in this work. Even though their CO_2 conversions were greater than the ones reported here, their finite selectivity to CH_4 caused their CO yields to be similar to the ones reported here. Y. Liu and D. Liu [16] noticed an increase in CH_4 when the Ni content of the CuNi catalysts was increased.

A comparison of the average CO yields for the carbon supported catalysts is shown in Figure 11. The CO yields obtained with $Cu_{50}Ni_{50}$/C catalyst are smaller than those obtained with the other two CuNi catalysts. The $Cu_{50}Ni_{50}$/C catalyst was the one that appeared to be compositionally stable according to the XPS results discussed previously. It was also the one that appeared to be the most thermally stable in Figure 4. Perhaps there is an association between minimum CO yield and thermal stability. In other words, perhaps the reaction sites on CuNi catalysts with the largest turnover frequencies are the ones that are the most thermally unstable. Thermal stability was further investigated and is discussed in another work [27]. Here, testing using $Cu_{50}Ni_{50}$ deposited on samarium-doped ceria showed no sign of deactivation when the catalyst is exposed to temperatures of 600–700°C for 48 consecutive hours. The high CO yields

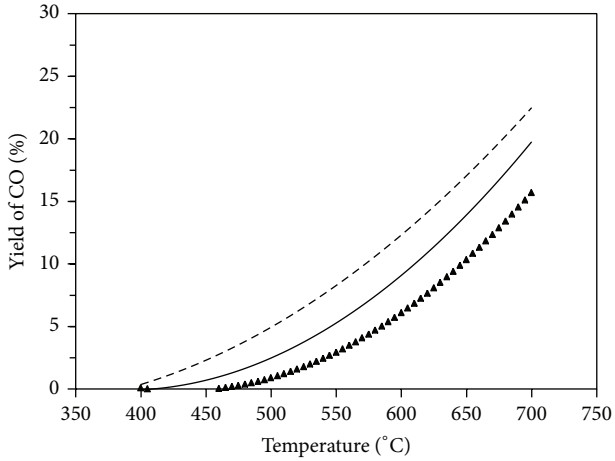

Figure 11: Average yield of CO for the reverse water gas shift reaction at 1 atm, $P_{H2} = P_{CO2} = 1$ kPa, balance He, GHSV = 176000 h^{-1}, and 50 mg of Cu_xNi_{1-x}/C catalyst: The solid line represents $Cu_{20}Ni_{80}$/C catalysts, the triangles represent $Cu_{50}Ni_{50}$/C catalysts, and the dashed line represents $Cu_{80}Ni_{20}$/C catalysts.

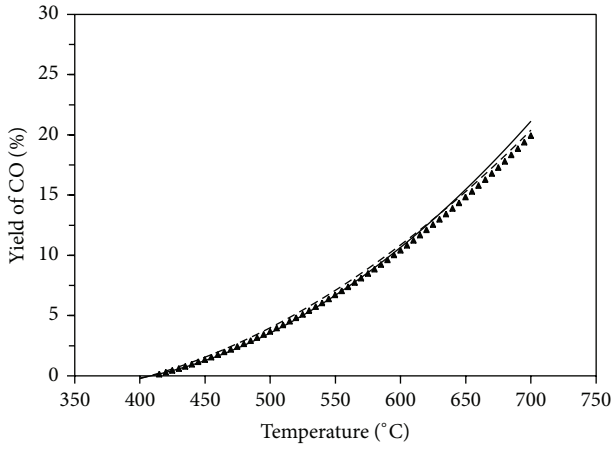

Figure 12: Average yield of CO for the reverse water gas shift reaction at 1 atm, $P_{H2} = P_{CO2} = 1$ kPa, balance He, GHSV = 282000 h^{-1}, and 50 mg of Cu_xNi_{1-x}/γ-Al_2O_3 catalyst: The solid line represents $Cu_{20}Ni_{80}/\gamma$-Al_2O_3 catalysts, the triangles represent $Cu_{50}Ni_{50}/\gamma$-Al_2O_3 catalysts, and the dashed line represents $Cu_{80}Ni_{20}/\gamma$-Al_2O_3 catalysts.

obtained using $Cu_{80}Ni_{20}$/C are believed to be associated with a high Cu concentration on the surface of the catalyst as shown in the XPS results. As mentioned previously, Cu is known to obtain higher CO yields than Ni for the RWGS reaction [16].

A comparison of the average CO yields for the alumina supported catalysts shown in Figure 12 is almost identical regardless of catalyst composition. Nevertheless substantial catalyst deactivation was evident in Figures 7–10. That suggests that the deactivation caused by thermal transitions in alumina (loss of surface area, spinel formation) may have had more influence on catalyst performance than variations in CuNi catalyst composition. In spite of the similarity of the results in Figure 12, the CO yields for the $Cu_{50}Ni_{50}/\gamma$-Al_2O_3 catalyst appear to be slightly less than the other two catalyst compositions. That is consistent with the observation in Figure 11 that the $Cu_{50}Ni_{50}$/C catalyst also produced smaller yields than the other two CuNi catalysts.

As discussed above, some deactivation occurs when CuNi metal is supported on either carbon or γ-Al_2O_3. As a result, most catalysts composed of CuNi metal supported on either carbon or γ-Al_2O_3 will not satisfy one of the main objectives of this research, namely, obtaining a thermally stable catalyst capable of operating under high temperatures. The one exception discussed here is the $Cu_{50}Ni_{50}$/C catalyst. Unless deactivation can be mitigated CuNi catalysts will not meet the requirements for an efficient, industrially viable catalyst.

4. Conclusion

The results of this investigation can be summarized by the following statements: The new polyol synthesis method permits both Cu and Ni metal salts to be reduced at the same time and at the same temperature, by first heating the Ni salt solution to 196°C and then adding the Cu salt solution that was at room temperature. In the past [18] a Ni rich surface was obtained because $Cu(NO_3)_2$ was reduced first at temperatures as low as 140°C followed by $Ni(NO_3)_2$ reduction as the solution continued to be heated to 196°C. Instead, a Cu rich surface is obtained which is ideal for the RWGS reaction because Cu has a higher selectivity towards CO than Ni. The CuNi alloy catalysts investigated in this work are similar to pure Cu catalysts in that they show selectivity for CO formation and the absence of CH_4 formation. The selectivity to CO was attributed to Cu being the most abundant metallic species on the surface of the catalyst, as determined by XPS measurements. Although some of the CuNi alloys show some deactivation, they are not nearly as thermally unstable as pure Cu (sintering) at the higher temperatures that are necessary for the equilibrium of the RWGS reaction to be thermodynamically favorable. Deactivation was observed in each case that an alumina catalyst support was used which was attributed to the instability of alumina at high temperatures. With one carbon supported catalyst, $Cu_{50}Ni_{50}$/C, there was no deactivation between the second and third temperature cycles and it appeared to be compositionally stable according to XPS and SEM results. Finally, CO yields at 700°C during the third temperature cycle of each CuNi catalyst were comparable to those with the Pt/C catalyst.

In conclusion, considering the difference in cost between CuNi alloys and Pt metal, these results suggest that more studies are warranted on the use of CuNi alloy catalysts for the RWGS reaction using the synthesis method described in this work.

Conflict of Interests

The authors declare that there is no conflict of interests regarding the publication of this paper.

Acknowledgments

The Natural Science and Engineering Research Council (NSERC) and Phoenix Canada Oil Company Limited are gratefully acknowledged for their financial support. The scientific contributions provided by Dr. Marten Ternan are also acknowledged.

References

[1] W. Wang, S. Wang, X. Ma, and J. Gong, "Recent advances in catalytic hydrogenation of carbon dioxide," *Chemical Society Reviews*, vol. 40, no. 7, pp. 3703–3727, 2011.

[2] P. Vibhatavata, J.-M. Borgard, M. Tabarant, D. Bianchi, and C. Mansilla, "Chemical recycling of carbon dioxide emissions from a cement plant into dimethyl ether, a case study of an integrated process in France using a Reverse Water Gas Shift (RWGS) step," *International Journal of Hydrogen Energy*, vol. 38, no. 15, pp. 6397–6405, 2013.

[3] S. S. Kim, K. H. Park, and S. C. Hong, "A study of the selectivity of the reverse water-gas-shift reaction over Pt/TiO_2 catalysts," *Fuel Processing Technology*, vol. 108, pp. 47–54, 2013.

[4] S. S. Kim, H. H. Lee, and S. C. Hong, "A study on the effect of support's reducibility on the reverse water-gas shift reaction over Pt catalysts," *Applied Catalysis A: General*, vol. 423-424, pp. 100–107, 2012.

[5] S. S. Kim, H. H. Lee, and S. C. Hong, "The effect of the morphological characteristics of TiO_2 supports on the reverse water-gas shift reaction over Pt/TiO_2 catalysts," *Applied Catalysis B: Environmental*, vol. 119-120, pp. 100–108, 2012.

[6] G. Pekridis, K. Kalimeri, N. Kaklidis et al., "Study of the reverse water gas shift (RWGS) reaction over Pt in a solid oxide fuel cell (SOFC) operating under open and closed-circuit conditions," *Catalysis Today*, vol. 127, no. 1–4, pp. 337–346, 2007.

[7] C. S. Chen, J. H. Wu, and T. W. Lai, "Carbon dioxide hydrogenation on Cu nanoparticles," *The Journal of Physical Chemistry C*, vol. 114, no. 35, pp. 15021–15028, 2010.

[8] C.-S. Chen, W.-H. Cheng, and S.-S. Lin, "Mechanism of CO formation in reverse water-gas shift reaction over Cu/Al_2O_3 catalyst," *Catalysis Letters*, vol. 68, no. 1-2, pp. 45–48, 2000.

[9] L. Wang, S. Zhang, and Y. Liu, "Reverse water gas shift reaction over Co-precipitated $Ni\text{-}CeO_2$ catalysts," *Journal of Rare Earths*, vol. 26, no. 1, pp. 66–70, 2008.

[10] F. S. Stone and D. Waller, "Cu-ZnO and $Cu\text{-}ZnO/Al_2O_3$ catalysts for the reverse water-gas shift reaction. The effect of the Cu/Zn ratio on precursor characteristics and on the activity of the derived catalysts," *Topics in Catalysis*, vol. 22, no. 3-4, pp. 305–318, 2003.

[11] J. Lin, *Supported Copper, Nickel and Copper-Nickel nanoparticle Catalyst for Low Temperature WGS Reaction*, University of Cincinnati, 2012.

[12] C. Chen, C. Ruan, Y. Zhan, X. Lin, Q. Zheng, and K. Wei, "The significant role of oxygen vacancy in Cu/ZrO_2 catalyst for enhancing water-gas-shift performance," *International Journal of Hydrogen Energy*, vol. 39, no. 1, pp. 317–324, 2014.

[13] C. S. Chen, W. H. Cheng, and S. S. Lin, "Study of reverse water gas shift reaction by TPD, TPR and CO_2 hydrogenation over potassium-promoted Cu/SiO_2 catalyst," *Applied Catalysis A: General*, vol. 238, no. 1, pp. 55–67, 2002.

[14] C.-S. Chen, W.-H. Cheng, and S.-S. Lin, "Study of iron-promoted Cu/SiO_2 catalyst on high temperature reverse water gas shift reaction," *Applied Catalysis A: General*, vol. 257, no. 1, pp. 97–106, 2004.

[15] C. S. Chen, J. H. Lin, J. H. You, and K. H. Yang, "Effects of potassium on $Ni\text{-}K/Al_2O_3$ catalysts in the synthesis of carbon nanofibers by catalytic hydrogenation of CO_2," *Journal of Physical Chemistry A*, vol. 114, no. 11, pp. 3773–3781, 2010.

[16] Y. Liu and D. Liu, "Study of bimetallic $Cu\text{-}Ni/\gamma\text{-}Al_2O_3$ catalysts for carbon dioxide hydrogenation," *International Journal of Hydrogen Energy*, vol. 24, no. 4, pp. 351–354, 1999.

[17] L. Poul, N. Jouini, and F. Fiévet, "Layered hydroxide metal acetates (metal = zinc, cobalt, and nickel): elaboration via hydrolysis in polyol medium and comparative study," *Chemistry of Materials*, vol. 12, no. 10, pp. 3123–3132, 2000.

[18] F. Bonet, S. Grugeon, L. Dupont, R. Herrera Urbina, C. Guéry, and J. M. Tarascon, "Synthesis and characterization of bimetallic Ni-Cu particles," *Journal of Solid State Chemistry*, vol. 172, no. 1, pp. 111–115, 2003.

[19] C. Bock, C. Paquet, M. Couillard, G. A. Botton, and B. R. MacDougall, "Size-selected synthesis of PtRu nano-catalysts: reaction and size control mechanism," *Journal of the American Chemical Society*, vol. 126, no. 25, pp. 8028–8037, 2004.

[20] G. Viau, F. Fiévet, and F. Fiévet-Vincent, "Nucleation and growth of bimetallic CoNi and FeNi monodisperse particles prepared in polyols," *Solid State Ionics*, vol. 84, no. 3-4, pp. 259–270, 1996.

[21] R. J. Isaifan, S. Ntais, and E. A. Baranova, "Particle size effect on catalytic activity of carbon-supported Pt nanoparticles for complete ethylene oxidation," *Applied Catalysis A: General*, vol. 464-465, pp. 87–94, 2013.

[22] R. J. Isaifan, H. A. E. Dole, E. Obeid, L. Lizarraga, E. A. Baranova, and P. Vernoux, "Catalytic CO oxidation over Pt nanoparticles prepared from the polyol reduction method supported on Yttria-Stabilized Zirconia," *ECS Transactions*, vol. 35, no. 28, pp. 43–57, 2011.

[23] H. A. E. Dole, R. J. Isaifan, F. M. Sapountzi et al., "Low temperature toluene oxidation over Pt nanoparticles supported on yttria stabilized-zirconia," *Catalysis Letters*, vol. 143, no. 10, pp. 996–1002, 2013.

[24] P. van der Plank and W. M. H. Sachtler, "Surface composition of equilibrated copper-nickel alloy films," *Journal of Catalysis*, vol. 7, no. 3, pp. 300–303, 1967.

[25] K. Watanabe, M. Hashiba, and T. Yamashina, "A quantitative analysis of surface segregation and in-depth profile of copper-nickel alloys," *Surface Science*, vol. 61, no. 2, pp. 483–490, 1976.

[26] T. Sakurai, T. Hashizume, A. Jimbo, A. Sakai, and S. Hyodo, "New result in surface segregation of Ni-Cu binary alloys," *Physical Review Letters*, vol. 55, no. 5, pp. 514–517, 1985.

[27] M. Lortie, *Reverse water gas shift reaction over supported Cu-Ni nanoparticle catalysts, chapter 3 [M.S. dissertation]*, University of Ottawa, 2014.

[28] M. V. Twigg and M. S. Spencer, "Deactivation of supported copper metal catalysts for hydrogenation reactions," *Applied Catalysis A: General*, vol. 212, pp. 161–174, 2001.

[29] R. K. Oberlander, "Aluminas for catalysts: their preparation and properties," in *Applied Industrial Catalysis*, vol. 3, p. 67, Academic Press, Orlando, Fla, USA, 1984.

[30] J. Hu, K. P. Brooks, J. D. Holladay, D. T. Howe, and T. M. Simon, "Catalyst development for microchannel reactors for martian in situ propellant production," *Catalysis Today*, vol. 125, no. 1-2, pp. 103–110, 2007.